SAND2013-7006C

Time-encoded imaging of energetic radiation

James Brennan, Erik Brubaker, Mark Gerling, Peter Marleau, Aaron Nowack, Patricia Schuster

Sandia National Laboratories, Livermore, CA

ABSTRACT

Time-encoded imaging (TEI) is a new approach to directional detection of energetic radiation that produces images by inducing a time-dependent modulation of detected particles. TEI-based detectors use single-scatter events and have a low channel count, reducing complexity and cost while maintaining high efficiency with respect to other radiation imaging techniques such as double-scatter or coded aperture imaging. The scalability of TEI systems makes them a very promising detector class for weak source detection. Extension of the technique to high-resolution imaging is also under study.

With a prototype time-encoding detector, we demonstrated detection of a neutron source at 60 m with neutron output equivalent to an IAEA significant quantity of WGPu. We have since designed and built a full-scale detector based on the time-encoding concept. We will present results from characterization of very large liquid scintillator cells, including pulse shape discrimination, as well as from studies of the detector system performance in weak source detection scenarios.

Keywords: Time-encoded imaging, neutron, SNM detection

1. INTRODUCTION

Detection of special nuclear material (SNM) in small quantities, at large distances, or under heavy shielding—generically the weak source detection problem—requires a radiation detection system that has large detection area and efficiency, and good signal-to-background discrimination. Directional information can provide the latter, since sources of interest are localized, in contrast to more diffuse or near-isotropic backgrounds. However, most approaches to directional radiation detection (coded aperture imaging, double-scatter imaging) involve complex systems, requiring many channels or expensive position-sensitive detection elements. We are developing an alternative approach using time-encoded imaging (TEI), which can use very large detection elements with enough directional sensitivity to discriminate a point-like signal from diffuse background.[1]

We have demonstrated the time-encoded imaging concept applied to standoff SNM detection with a prototype system and with simulated results, which will be described briefly in Sec. 2. In order to take full advantage of the TEI approach for SNM detection via the fast neutron signature, we have investigated the use of large liquid scintillator (LS) cells as TEI detection elements. Various cell configurations were studied, primarily using different photomultiplier tube (PMT) candidates. Scintillation light collection from the cell and PMT characteristics were identified as the most important variables. The comparisons between different cell configurations, focused on their pulse shape discrimination (PSD) performance, are described in Sec. 3. Finally, the selected cell configuration, a 11"D x 15" LS volume coupled to three 5" PMTs, was characterized. The cell's energy scale calibration, PSD performance, and sensitivity to the position of interaction are detailed in Sec. 4.

2. TIME-ENCODED IMAGING SYSTEM

Time encoded imaging (TEI) is an approach to directional detection that produces images by inducing a time-dependent modulation of detected particles. TEI-based detectors use single-scatter events and have a low channel count, reducing complexity and cost while maintaining high efficiency with respect to other radiation imaging techniques such as double-scatter or coded aperture imaging. The scalability of TEI systems makes them a very promising detector class for weak source detection.

E. Brubaker: ebrubak@sandia.gov

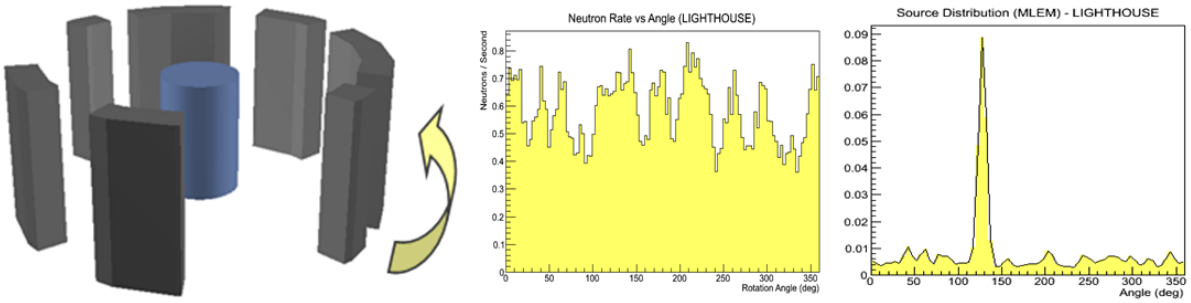

Figure 1. One-dimensional fission-energy neutron imaging using a time-encoded imager prototype. Left: simplified schematic of the prototype as built. The passive HDPE mask elements (black) rotate around the central detector (blue). Center: The neutron rate as a function of time (or equivalently angle of mask rotation), demonstrating the characteristic modulation for background plus a nearby point source. Right: MLEM reconstruction of the source distribution in azimuth, identifying the point source location.

We have focused on fast neutron detection and imaging using TEI since directional information is relatively more important for signal-to-background discrimination in the case of neutrons than it is for gammas. Briefly, in time-encoded neutron imaging, a time modulation of a detected neutron signal is induced—for example, a moving mask that attenuates neutrons with a time structure that depends on the source position. Time-encoded imaging is in many ways analogous to coded aperture imaging; the *spatial* modulation of a particle flux induced by a fixed mask on a *position-sensitive image plane* is replaced by the *time* modulation of a particle flux induced by a moving mask on one or a few *time-sensitive detectors*.

Figure 1 demonstrates the TEI concept for a system based on a passive rotating mask, sensitive to source position in one dimension (azimuthal). For SNM search in many environments, azimuthal sensitivity is sufficient to detect a source, which would typically located near the horizon at some distance.

2.1 PRISM prototype

By operating in the time domain, a different set of directionally sensitive detector systems can be considered. The weak source detection application (large standoff, small quantities of SNM, and/or heavy shielding) is likely to be a signal-starved scenario, so one would like a detector system with a very large active volume.

The Portable Rotating Imager using Self Modulation (PRISM) prototype is composed of three large detectors cells, as shown in Fig. 2 (left), each serving as an active shield for adjacent cells as they rotate around a common central axis. Although the PRISM design has low angular resolution for source location, it is highly scalable scalable; an order of magnitude more active scintillator volume can be used in a PRISM design than in the design of Fig. 1 for similar size, weight, and cost constraints.

In the PRISM detector, a localized source on the horizon will show a characteristic time modulation in each detector due to the shadow induced by the other detectors passing through the line of sight to the source. Figure 2 (right) shows the expected modulation patterns, determined using MCNP, for a given source location. In order to identify the presence of a localized source, we perform a hypothesis test that involves the likelihood ratio between a signal-plus-background hypothesis and a uniform-background-only (no time modulation) hypothesis. Since the location of the source is unknown *a priori*, the source position and strength that results in the largest likelihood ratio is used. If the likelihood ratio exceeds a threshold determined in advance for the measurement, we conclude that a source is present.

Although only one of the three cells in the prototype was active, detection of a ^{252}Cf source with neutron rate equivalent to an IAEA significant quantity of weapons-grade plutonium (WGPu) was demonstrated at 60 m. After 1.3 hours of dwell time, the source could be clearly identified by the difference between background-only and signal-added data, which has the expected time modulation, as shown in Fig. 3. However, there is also a modulation in the background-only data, which was traced to geomagnetic fields affecting the PMT gain as the system rotates. Additional magnetic shielding was installed and subsequent tests showed a flat background shape as expected for a typical environment.

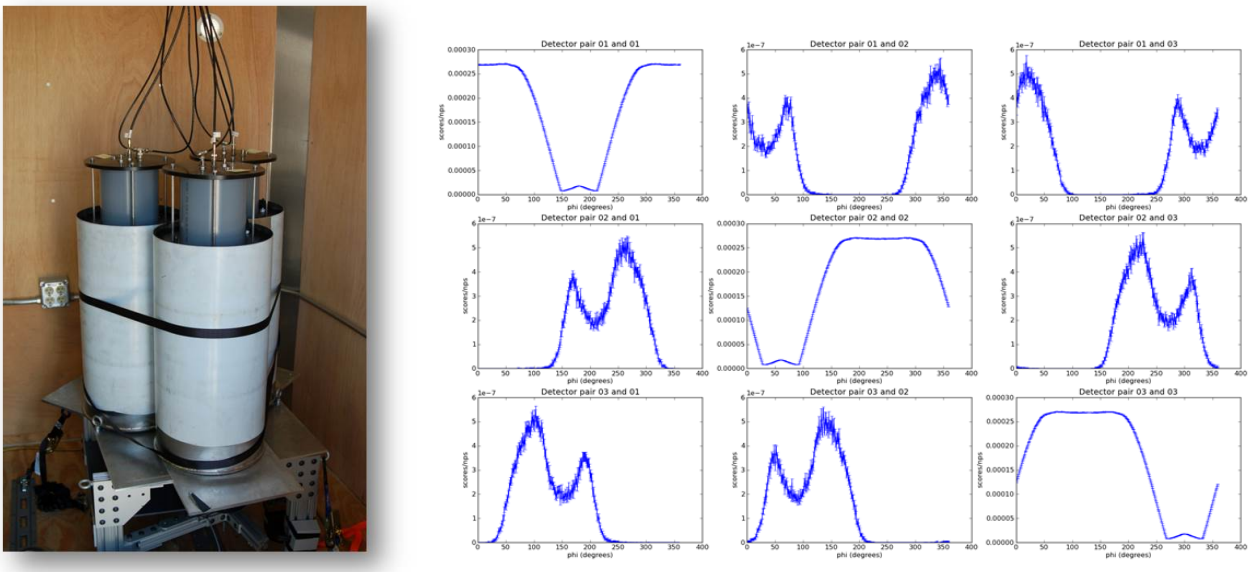

Figure 2. Left: The PRISM prototype, consisting of three large (27 L) liquid scintillator cells rotating around each other. As the system rotates, each cell is attenuated by the others for a given source location in azimuth. Right: The detected neutron rate (as simulated in MCNP) for a particular source location, where the three plots on the diagonal show the singles rate in each detector. These shapes are identical, but offset by a phase due to their different locations on the turntable. The off-diagonal plots show the rates of interactions in two cells as a function of turntable position; these events, however, are orders of magnitude less frequent.

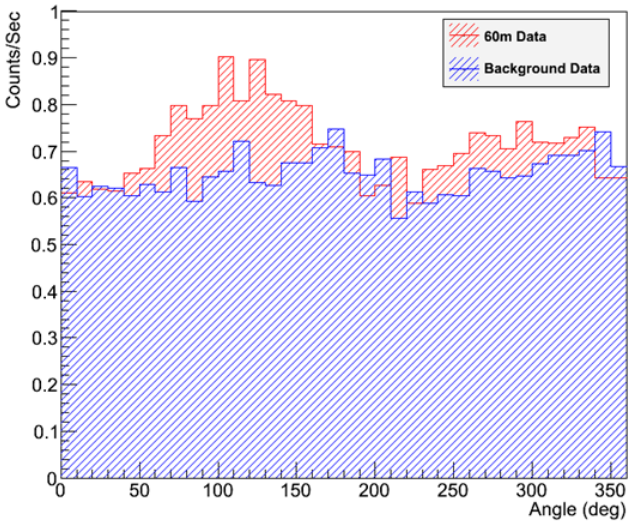

Figure 3. Results from an experimental test of the prototype PRISM system with a ^{252}Cf source at 60 m with neutron rate similar to an IAEA significant quantity of WGPu. The difference between datasets with and without source present is clear. Modulation in the background-only data was eliminated by additional magnetic shielding against geomagnetic fields.

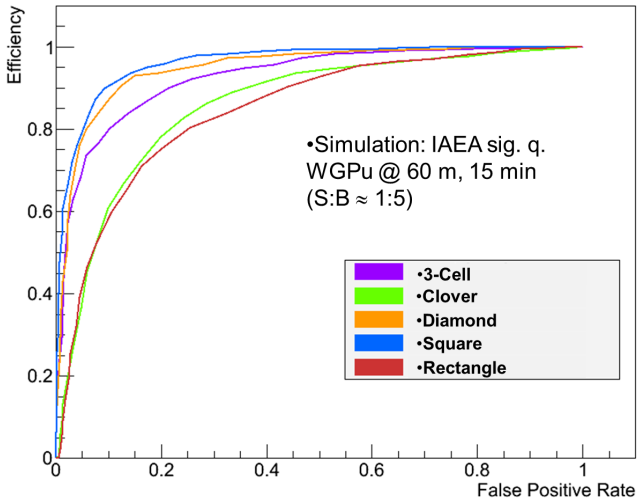

Figure 4. Simulated results from an upgraded PRISM 2.0 detector, currently in the integration phase. ROC curves for WGPu detection at standoff are shown for various arrangements of the three or four scintillator cells on the turntable.

2.2 PRISM 2.0 system

Given promising results with the prototype detector and associated simulations, we have designed and built a "PRISM 2.0" detector system with more robust construction and four active large LS cells. Figure 4 shows results from simulations of this larger system, which has an active LS volume of almost 100 L. The simulations assume a lower effective neutron threshold than in the prototype. Each curve is a receiver operator characteristic (ROC) curve for detection of an IAEA significant quantity of WGPu at 60 m in 15 min. Different curves correspond to different cell arrangements on the turntable, showing that the arrangement of the cells, and thus the attenuation response pattern, has a significant effect on detection.[2]

The limiting feature of the PRISM prototype was the performance of the large LS cell, in particular its ability to discriminate gamma from neutron events at low energies. In the rest of this submission, we detail our efforts and investigations to optimize PSD performance on large liquid scintillator cells to enable a highly sensitive standoff SNM detector system based on the TEI principle.

3. LARGE CELL COMPARISONS

With the goal of maximizing cell size while maintaining good performance, we studied several candidate large LS cell configurations.

3.1 Approach

Put simply, we would like to maximize the effective area of the detector for fission-energy neutrons, with a constraint on overall cost and complexity. Effective area is defined as the product of the physical cross-sectional area of the detector and its efficiency, which for fast neutrons in LS includes the probability of the particle interacting in the cell in a detectable way, and the probability that the neutron interaction can be distinguished from much more frequent gamma interactions via PSD.

For a given LS cell shape—right circular cylinder cells are the most common—the area and interaction probability scale with the detector size.* On the other hand, unless special care is taken to maintain good light collection efficiency, the PSD performance tends to decrease as the cell size increases. At some detector size comparable to the light attenuation length, insurmountable problems with photostatistics and time dispersion preclude effective PSD.

*The combined scaling is with the volume of the detector, i.e. $\epsilon_n \propto \ell^3$, for small detectors, but when the linear dimension reaches several interaction lengths ($\lambda = O(5\text{ cm})$) neutrons are unlikely to pass through the detector without interacting, and the scaling is closer to $\epsilon_n \propto \ell^2$.

As a metric for PSD performance, we define an effective threshold for neutron detection. This is the electron equivalent energy at which 90% of neutrons can be identified while rejecting 99.99% of gamma events. These are of course arbitrary values for desired neutron efficiency and gamma rejection, but driven by potential gamma/neutron ratios for a weak source of $O(10^4)$. The PSD parameter is defined using a ratio of the integrals of the tail of the pulse and the full pulse. The "tail" and "total" windows are defined by inspection for a given cell/PMT configuration.

3.2 Candidates

We investigated LS cells on a 12" scale—significantly larger than workhorse 5" cylindrical cells, but safely smaller than the light attenuation length in our scintillator of choice, EJ-309, which is quoted by the manufacturer as "$>$ 1 m".[3]

- A 12"D x 15" prototype LS cell (27 L active volume) with a single Photonis 9" XP1802 PMT immersed directly in the scintillator. Of the three cells we built of this type, only one demonstrated reasonable performance. We attribute the poor results on the other cells to problems with the aging PMTs and/or bases.
- A more robust 11"D x 15" (23 L) cell design was used for the remaining configurations. The first PMT tried was a 10" Hamamatsu R1950, also immersed in the LS. Optimized for low-light photon counting, this PMT had poor linearity and afterpulsing, resulting in poor PSD performance.
- Since the Hamamatsu H6527 PMT (5"D photocathode) is known to have good properties for PSD analysis (low afterpulsing, good gain, good timing), we tested the 11"D x 15" cell with an H6527 interfaced via a window and optical grease. This configuration suffered from poor light collection due to the small ratio of PMT photocathode area to the surface area of the cell.
- A second configuration with the H6527 used a 4" tapered light guide, intended to reduce the dependence of light collection on the position of interaction within the cell. Overall, however, the results were similar to or slightly worse than the previous candidate, i.e. phototstatistics limited.
- Finally, three H6527 PMTs were used on a single cell, all mounted on the top surface. The signal in the three PMTs was summed after gain matching to produce a single analyzable pulse per event. In this configuration, reasonable light collection and good PMT performance combined to provide acceptable PSD, as shown below.

4. FINAL CELL CHARACTERIZATION

Based on results in the previous section, we selected a 11"D x 15" cell with three 5" PMTs to build a demonstration TEI/PRISM system for standoff SNM detection. Here we describe a more complete characterization of the cell performance.

As a first step, the gains of the three PMTs were normalized by adjusting the HV supply to each PMT until they produced the same pulse height spectrum for a Cs-137 source placed directly under the center of the cell, opposite and equidistant from the three PMTs.

4.1 Variations with interaction location

Since there are three PMTs, resulting in an azimuthal asymmetry in the detector, and consistency of the azimuthal response is extremely important for the PRISM concept, we first checked for any dependence in the energy scale on the location of a gamma source.

A Cs-137 source was located at the vertical midpoint ($z = 7$ in) of the cell, about 5 cm from the surface of the cell. Data was acquired for azimuthal locations of the source starting directly in line with the first PMT and continuing at 20^o intervals around the circumference to the opposite side of the cell. Figure 5 (left side) plots the resulting pulse height spectra, showing no azimuthal dependence of the detector energy response. A

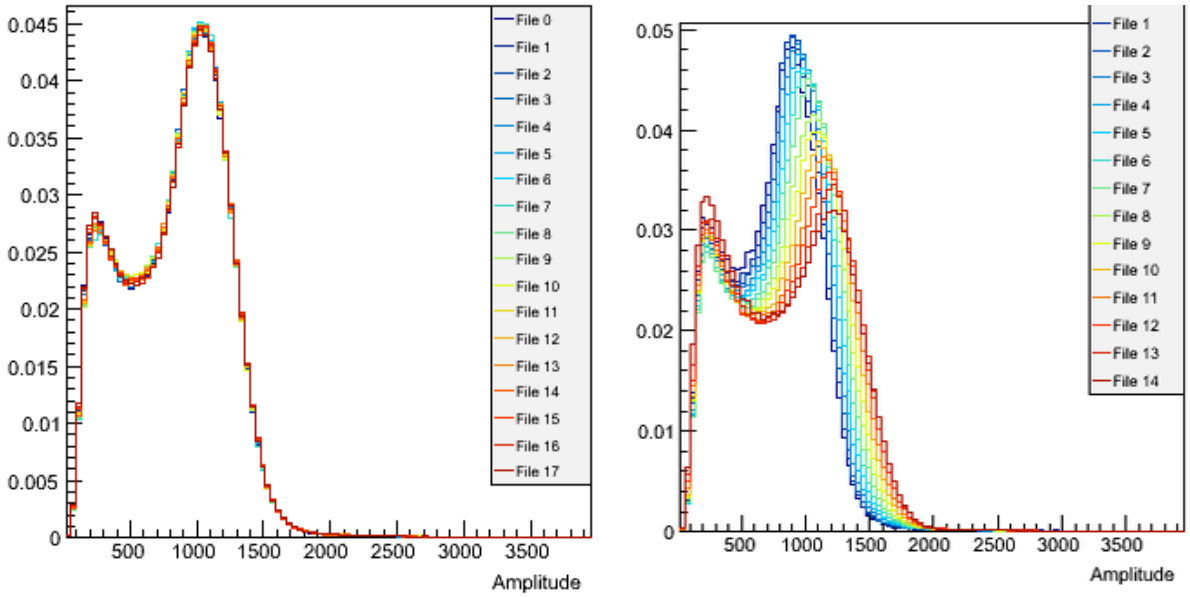

Figure 5. Pulse height spectra for runs with Cs-137 located at various positions around the cell. The left plot shows 18 runs scanning the source position through azimuthal positions around half of the circumference of the cell, with z fixed. No dependence on source azimuthal location is observed. The right plot shows 15 runs scanning the source through a range of z positions with ϕ fixed. A significant dependence on z is observed, due to reduced light collection when the interaction occurs farther from the PMTs.

tungsten collimator was also used to more precisely probe interaction locations within the cell, but it was found that downscattering in the collimator washed out the Compton edge location and made the comparison difficult.

There is also expected to be a variation in the light collection as a function of the interaction z position. This dependence was characterized by placing the Cs-137 source about 5 cm from the surface of the cell, at a range of z positions from the bottom of the cell (run 0) to the top (run 15), with the azimuthal position fixed to the ϕ of the first PMT. For each run the source was raised by 1". Figure 5 (right side) shows the resulting spectra. There is clearly a dependence, but this is not a significant concern, both because it does not interact with the time encoding (as a function of turntable rotation) and because a source on the horizon at distance greater than a few times the detector height will interact roughly uniformly in the detector volume.

4.2 Energy calibration

An energy calibration was performed to convert measured amplitude to electron equivalent energy. A Na-22 source (with 511 keV and 1.2 MeV gamma lines) was placed at the side of the cell, vertically centered and 5 cm from the cell surface. The acquired amplitude spectrum can be fitted to the expected deposited energy distribution from a Monte Carlo simulation of a similar geometry. The results are shown in Fig. 6. Note the presence of a full-energy peak for each gamma line in the blue deposited energy curve, since many gammas interact multiple times in the large volume and are fully absorbed. The full-energy peak, the Compton edge, and the region between cannot be resolved after resolution effects are taken into account (black points representing the data, and red curve representing the Monte Carlo distribution after applying gain and resolution effects). The fitted gain parameters are used to convert the measured amplitude of events to their electron-equivalent energy.

4.3 PSD calibration

A dataset for PSD calibration was acquired using an AmBe source, providing a mix of gamma and neutron events at a range of deposited energies. (See Fig. 7.) In order to characterize the PSD distributions, the amplitude range is divided into bins; in each bin the PSD parameter forms a bimodal shape, with one peak representing gamma

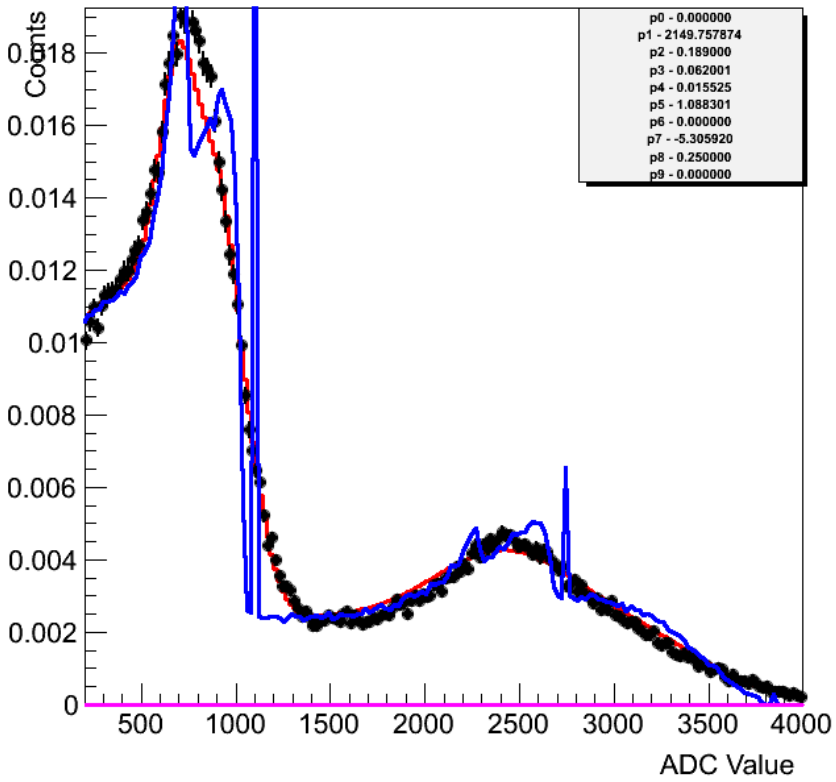

Figure 6. This figure shows the result of energy calibrations using a Na-22 source placed 5 cm from the surface of the cell halfway up. Black points are the acquired spectral data, the blue curve is the distribution of energy deposited predicted by a Monte Carlo simulation, and the red curve is the result of a fit to several gain, resolution, and low-energy background parameters. The fitted low-energy background curve is represented by the purple line. For display purposes, the blue MC curve has been converted to the amplitude scale according to the fitted gain parameters.

events with smaller PSD parameter, and the other representing neutron events with larger PSD parameter. Each such slice of the PSD distribution is fitted to a double Gaussian shape, and the resulting parameters are stored for each pulse amplitude bin. These parameters can be used to determine the relative likelihood of a given event being from the neutron or the gamma distribution, or to generate appropriate PSD parameter values for a simulated event. The right side of Fig. 7 shows the neutron identification efficiency (fraction of the neutron peak to the right of a cut value) for PSD cuts defined (as a function of pulse amplitude) to reject 99.99% of the events in the gamma peak at each amplitude. For this cell, the energy at which 90% of neutron events can be identified while rejecting 99.99% of gamma events is $\sim$ 250 keV.

5. CONCLUSION

The effective threshold of 250 keV for our large LS cell, although certainly higher than the comparable value for smaller cells with larger fractional photocathode coverage, combines with the large physical area and volume of this cell to make a detector with quite large effective area for fission-energy neutrons. This cell enables a highly sensitive standoff SNM detector system based on time-encoded imaging.

ACKNOWLEDGMENTS

Sandia National Laboratories is a multi-program laboratory managed and operated by Sandia Corporation, a wholly owned subsidiary of Lockheed Martin Corporation, for the U.S. Department of Energy's National Nuclear Security Administration under contract DE-AC04-94AL85000.

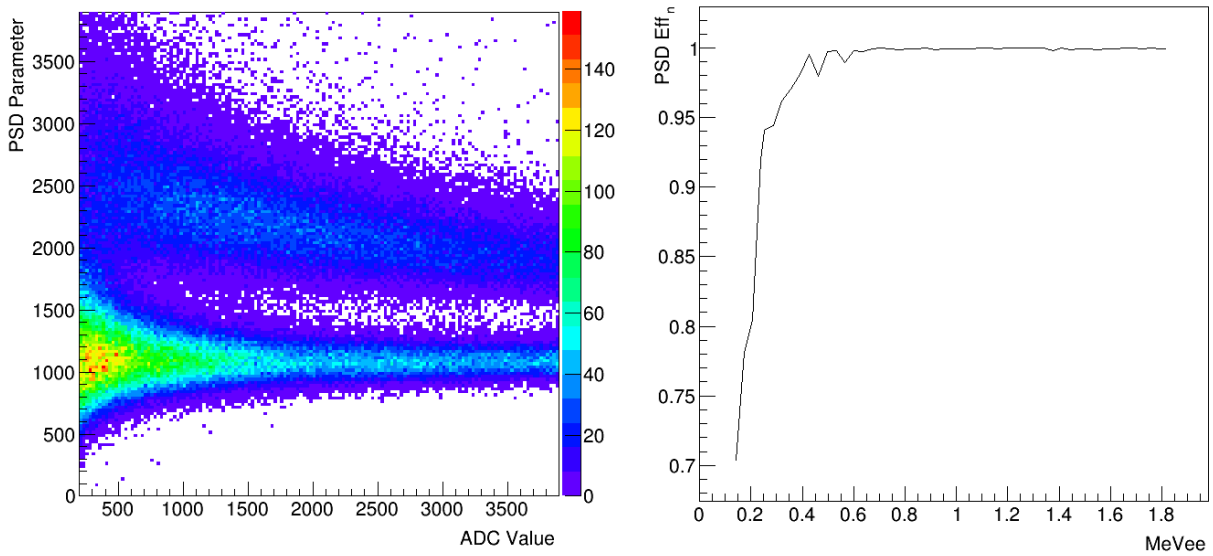

Figure 7. Left: Two-dimensional distribution of PSD parameter (two-window method) vs amplitude for pulses in an AmBe calibration dataset. Right: Using the fitted double Gaussians as described in the text, we determine the neutron identification efficiency for a PSD cut that rejects 99.99% of gamma events at each amplitude. The neutron ID efficiency is plotted as a function of the electron-equivalent energy, calculated from the amplitude using the energy calibration of Sec. 4.2.

REFERENCES

[1] Marleau, P., Brennan, J., Brubaker, E., Gerling, M., Nowack, A., Schuster, P., and Steele, J., "Time encoded fast neutron/gamma imager for large standoff SNM detection," in [*2011 IEEE Nuclear Science Symposium Conference Record*], 591–595, IEEE (Oct. 2011).

[2] Nowack, A., Brennan, J., Brubaker, E., Gerling, M., Marleau, P., Mcmillan, K., Schuster, P., and Steele, J., "Fast Neutron Time Encoded Imaging for Special Nuclear Material Detection," in [*Proceedings INMM 53rd Annual Meeting*], (2012).

[3] `http://www.eljentechnology.com/index.php/products/liquid-scintillators/73-ej-309`. Accessed: 2013-08-01.